Macromolecules

ARTICLE

pubs.acs.org/Macromolecules

A Phase Diagram of the P3HT:PCBM Organic Photovoltaic System: Implications for Device Processing and Performance

Paul E. Hopkinson,*,† Paul A. Staniec,‡ Andrew J. Pearson,‡ Alan D. F. Dunbar,§ Tao Wang,‡ Anthony J. Ryan,⊥ Richard A. L. Jones,‡ David G. Lidzey,‡ and Athene M. Donald*,†

†Cavendish Laboratory, Department of Physics, University of Cambridge, Cambridge CB3 0HE, U.K.

‡Department of Physics and Astronomy, University of Sheffield, Hicks Building, Hounsfield Road, Sheffield S1 3RH, U.K.

§Department of Chemical and Biological Engineering, University of Sheffield, Sheffield S1 3JF, U.K.

⊥Department of Chemistry, University of Sheffield, Sheffield S3 7HF, U.K.

Supporting Information

ABSTRACT: This paper describes the construction of a phase diagram for the as-cast state in the organic photovoltaic system P3HT:PCBM. Evidence for a transition to a phase-separated state at PCBM concentrations greater than 70 wt % is seen both by DMTA and GIWAXS, and the glass transition temperatures of blends in the single phase state below 70 wt % PCBM are observed to be raised compared to the pure polymer. Pure PCBM is observed to exhibit a thermal transition at 155 °C, an observation unreported to date—offering insight into crystallites commonly seen in device films. The liquid-crystal phase of P3HT is shown to persist in the presence of up to 41 wt % PCBM. In addition, pure PCBM is shown to be significantly hygroscopic, with important implications for the processing of high-performance devices.

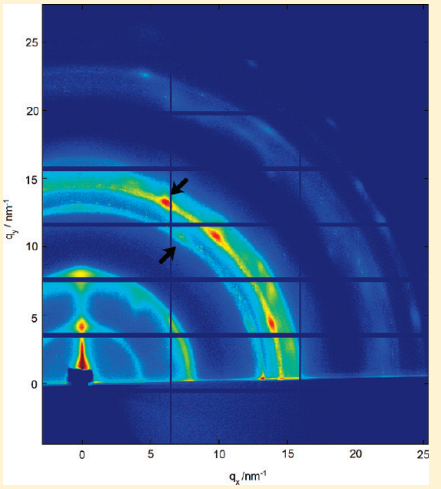

INTRODUCTION

With increasing pressure to reduce dependence on fossil fuels, renewable energy sources are attracting considerable interest. Organic photovoltaics are one particular class of materials which offer a number of benefits over conventional silicon cells, including the possibility of large-scale inexpensive production on flexible substrates and significantly lower capital cost.[1]

Poly(3-hexylthiophene) (P3HT), [6,6]-phenyl-C_{61}-butyric acid methyl ester (PCBM) blend solar cells have attracted a great deal of interest over the past 5 years,[2−6] being routinely used to produce photovoltaic devices with efficiencies 4−5%.[7−9] It has become clear that optimized morphology is crucial for good photovoltaic performance[2,4,10−12] and that annealing treatments, particularly thermal annealing, can substantially improve the performance of devices by altering both the phase separation and crystallinity of the films.[13,14] Such annealing treatments have so far been determined empirically, with a wide range of reportedly optimized treatments[2,5,9,11,15] but no underpinning rationale. Understanding the thermal properties of these materials should facilitate the development of optimization routes and rationalize some of the most effective strategies.

Within the reports of thermal properties of the polymer, there are conflicting measurements of the glass transition temperature (T_g), with values of −14, −3, 5.8, 12, 12.1, and 110 °C all reported[15−20] from differential scanning calorimetry (DSC) measurements. The difficulty in measuring the glass transition by DSC in a semicrystalline polymer such as P3HT likely contributes to the disagreement, and quenching or cooling from elevated temperatures has been used in all previous reports to ensure good thermal contact between the sample and the calorimeter. Such differences in the thermal history, which may change the measured T_g, are likely causes of some of these differences, in addition to variations in polymer properties such as molecular weight and regioregularity. Kuila and Nandi[21,22] have reported the use of dynamic mechanical thermal analysis (DMTA) to measure T_g in P3HT, with loss-modulus peaks at −16 and 24.4 °C, for as-cast and melt-quenched samples, respectively.

Received: November 6, 2010
Revised: February 1, 2011
Published: March 15, 2011

Phase diagrams for P3HT:PCBM blends have been previously reported by three sets of authors,[16,20,23] all from DSC measurements. Zhao et al.[20] and Kim and Frisbie[16] both observe continuous increases in the glass transition of the blends with increasing PCBM fraction, although Kim and Frisbie do not observe a glass transition above 75 wt %. Zhao et al. observe this trend to continue to 100 wt % PCBM. Kim and Frisbie's wide-angle X-ray scattering (WAXS) data indicated a solubility limit of PCBM in P3HT at 50 wt % PCBM for as-cast films and 30 wt % for thermally treated films. Field effect transistor measurements indicated hole-only transport below the solubility limit, with ambipolar transport at higher PCBM fractions. Zhao et al. showed the cold crystallization of both pure PCBM—at 159 °C—and of blends with more than 80 wt % PCBM. In contrast, Müller et al.[23] reported a eutectic phase diagram for the P3HT:PCBM system, with a eutectic composition of 35 wt % PCBM. While this was not reported by the other authors, Kim and Frisbie report similar melting temperature trends. We note that all the previous reports show thermal changes in the blends at 60−75 wt % PCBM, indicating that there is likely to be some important change in the blend structure in this composition range.

In this paper we report the application of an alternative technique to DSC—dynamic mechanical thermal analysis (DMTA)—to study the phase diagram of P3HT:PCBM. This method offers greater sensitivity to the glass transition than DSC and allows thermal analysis of samples without any heating prior to analysis. The thermal history is thus a much better model for spin-coating—the predominant method used in the production of research devices—or inkjet printing and other mass production techniques. Thus, the data we present here are more relevant to the production of devices. DMTA measures the storage and loss moduli of a sample under a dynamic force as a function of time or, as we report here, temperature. Changes in these properties can be observed as the sample undergoes a thermodynamic transition; for example, melting is observed as a rapid drop in storage modulus (stiffness) as the sample passes through the melting temperature.

We see evidence for phase separation of these materials at PCBM concentrations above 70 wt % by following both the bulk glass transition and melting temperatures. Grazing incidence wide-angle X-ray scattering (GIWAXS) shows significant structural differences between low and high wt % PCBM blends, further supporting a phase-separated state at high PCBM concentrations. In addition, we report the significant hygroscopicity of PCBM and a previously unreported transition of PCBM that occurs at typical device production temperatures.

RESULTS AND DISCUSSION

MALDI-TOF indicates that the P3HT used had a M_w of 8086 g mol^{-1}, M_n of 6705 g mol^{-1}, and a PDI of 1.21. Corresponding measurements from GPC are 13 510, 10 130 and 1.33 for M_w, M_n, and PDI, respectively. GPC correlates the hydrodynamic volume of a randomly coiled polymer with the molecular weight. Conjugated polymers such as P3HT, however, adopt a more rodlike conformation in solution; thus, the results by GPC are 1.5−2.0 times higher than by MALDI, as we find here and has been previously reported.[24]

A DMTA temperature scan of as-received P3HT powder is shown in Figure 1, with peaks in tan δ observed at 45 and 50 °C for 1 and 10 Hz, respectively. Second-order transitions have a strain frequency dependent temperature onset, unlike first-order

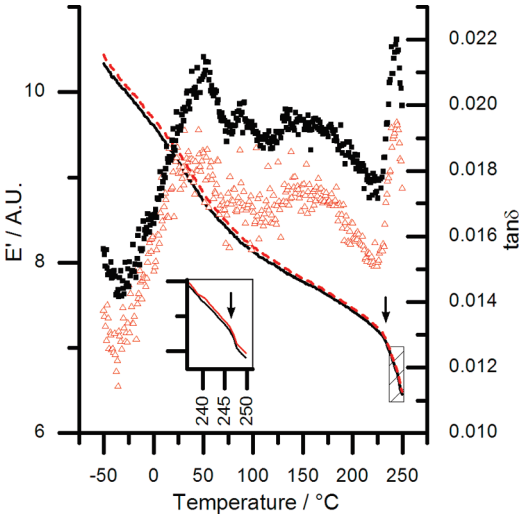

Figure 1. DMTA trace of as-received P3HT. The inset box shows the liquid-crystal melting on an expanded scale. Peaks in tan δ at 45 and 50 °C for 1 and 10 Hz, respectively, indicate T_g. The reductions of storage modulus at 233 and 246 °C show melting, first into a liquid-crystal state (indicated with an arrow in the main figure) and subsequently completely melting (indicated with an arrow in the inset). 1.0 Hz: E', black line; tan δ, black squares. 10 Hz: E', red dashed line; tan δ, red triangles.

phenomena, and this is also true of the glass transition. In the absence of second-order transitions at lower temperatures, and as this transition is likely to be the limiting factor in the processing of devices, we will label this transition T_g. While we have used a number of frequencies during temperature scans to aid in transition identification, we will use 1 Hz data for measurement of the glass transition temperature and the peak of tan δ as the T_g (in common with other DMTA reports[21,22,25,26]).

The glass transition temperature we have measured using DMTA at 1 Hz of 45 °C is somewhat higher than the most widely reported DSC value of 12 °C.[18,19] The main reason for this difference is likely to be that the T_g measured by DMTA is dependent upon the applied strain frequency, and measurement at very low frequencies results in unacceptably slow heating rates—thus annealing the sample substantially during the heating process. For comparison, the T_g of pure poly(vinyl chloride) is 82 °C by DSC (10 °C/min heating, typical for DSC) and 91 °C by DMTA (5 °C/min heating, 1 Hz strain frequency). The molecular weight of the polymer could also contribute to the difference between the T_g we report here and previous reports: we have observed that P3HT with 30% lower M_w has a T_g approximately 12 °C lower than the material we have used here (data not shown here).

Melting is indicated by a step drop in the storage modulus independent of strain rate. For pure P3HT two melting transitions are observed: with onsets at 233 and 244 °C (Figure 1). These two melting transitions that we observe in pure P3HT likely indicate the formation and melting of a liquid crystalline phase, as has been previously reported.[17,27,28] The magnitude of the transition from the liquid-crystal phase to the melt in the mechanical measurement is small, likely due to large-scale cooperative motion in the liquid-crystal phase.

Two DMTA scans of solvent-cast pure PCBM are shown in Figure 2. Below ambient temperature (5, 7 °C at 1, 10 Hz, respectively) peaks are observed in tan δ, indicating a second-order transition (Figure 2 a). This transition had poor reproducibility

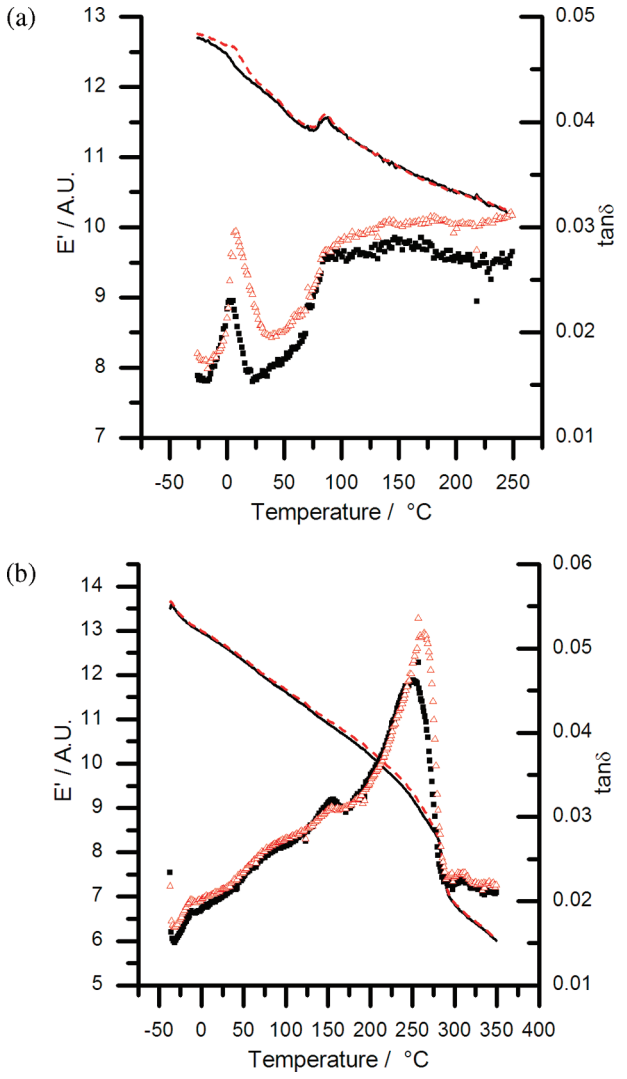

Figure 2. DMTA of pure solvent-cast PCBM: (a) showing the second-order transition A at 5 °C (1 Hz) and cold-crystallization at 79 °C; (b) showing first-order softening with an onset at 273 °C. 1.0 Hz: E', black line; tan δ, black squares. 10 Hz: E', red dashed line; tan δ, red triangles.

between samples, with transitions of a first-order nature observed at −12 and −3 °C (not shown here). Also observed in this DMTA thermal scan is the increase in storage modulus at 79 °C, likely to be due to cold crystallization. In Figure 2b the scan extends to higher temperatures: this allows us to observe the melting of the PCBM with an onset of 273 °C. Although the onset of this transition is a little lower than the previously reported values,[16] we attribute this to the formation of low quality crystals during the solvent-casting; our experiments show this transition is shifted with prolonged annealing (see below) to match those observed by others.

In the absence of other second-order transitions at higher temperatures, we postulate that the tan δ feature observed in pure PCBM by DMTA at 5 °C (1 Hz) is the glass transition of PCBM and that the transitions at −12 and −3 °C are attributable to motion of the side chain of the molecule. As these temperatures are significantly below ambient conditions, they have little relevance to photovoltaic device processing and have not been investigated in depth so far.

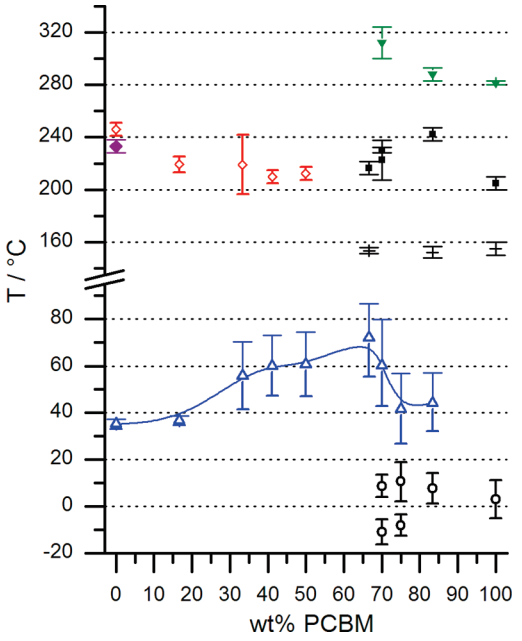

Figure 3. Phase diagram of P3HT:PCBM system from solvent-cast material, obtained from DMTA. The range of T_g (Δ) is shown with bars. The drop in the glass transition temperature of the blend observed between 70 and 75 wt % PCBM indicates phase separation. In addition, the transition at 154 °C (+) that is attributed to pure PCBM is not observed at fractions below 66 wt %, indicating that there is no free PCBM. Symbols: transition A (○); blend T_g (Δ); blend T_m (◇); transition B (+); transition C (■); transition D (▼); P3HT liquid-crystal transition (◆).

It is possible that the film casting process results in a cocrystal, as reported by Rispens et al.,[29] and that the transitions we observe are associated with such a cocrystal. However as the preparation of samples for DMTA is matched as closely as possible to device production, the transitions we observe in PCBM and P3HT:PCBM blends (see below) are likely to be relevant to the fabrication of photovoltaic devices.

Thermogravimetric analysis of PCBM (see Figure S1 in Supporting Information) shows that the powder is significantly hygroscopic: powder that had been subject to extended atmospheric exposure exhibited 10% mass loss at 100, indicating the loss of water. Further loss commences at 400 °C, indicating the breakdown of the molecule, with 57% of the sample mass remaining at 1000 °C.

Results from DMTA experiments (sample data in Figures S2−S4) using a range of P3HT:PCBM compositions enabled the construction of a phase diagram for the P3HT:PCBM system (Figure 3). The glass transition (represented by the Δ symbol in Figure 3) is shown to rise to between 58 and 72 °C at PCBM concentrations between 33 and 70 wt %, while at 16 wt % the glass transition of the blend is similar to that of the pure P3HT. Blends with PCBM concentrations above 70 wt % have a glass transition temperature similar to that at 16−33 wt %. The tan δ transitions (which we label A) observed between −10 and 10 °C in pure PCBM are also observed in blends composed of 75 wt % or more PCBM. Subtle first-order transitions (which we label B) are observed as a change in the gradient of the storage modulus for blends with PCBM concentrations of 66 wt % and above. By considering the intersection of the lines of best fit to the storage modulus either side of the transition, we obtain a characteristic temperature for the transition, with a mean value of 154 °C. This

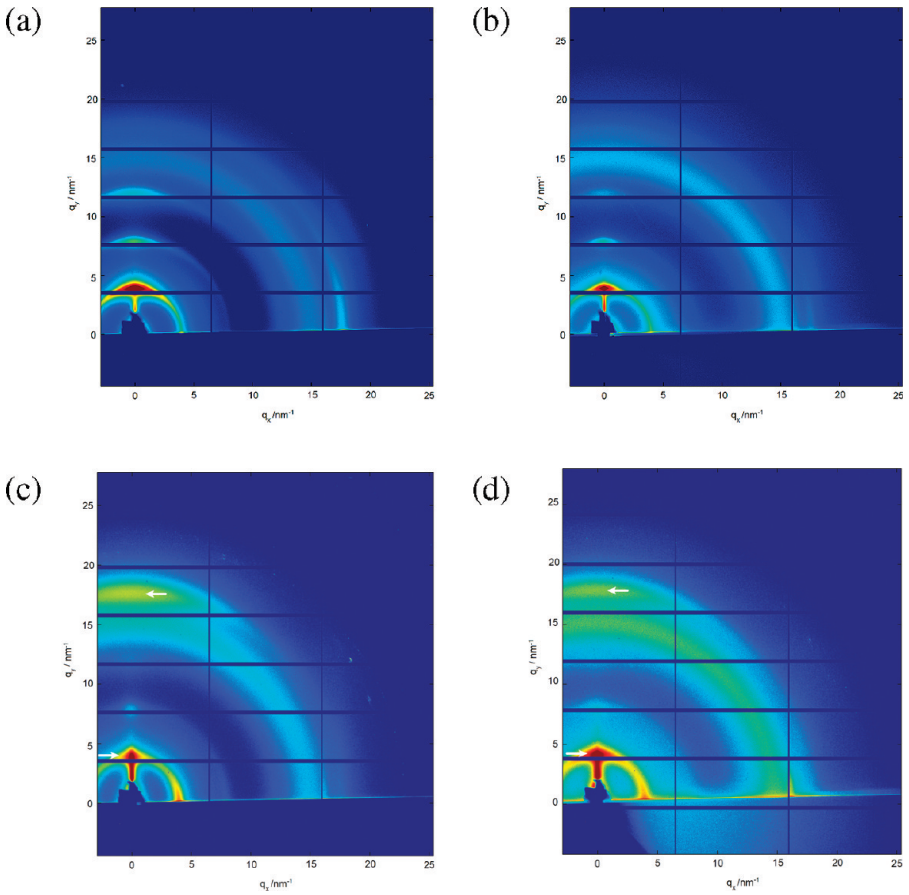

Figure 4. 2D GIWAXS images of spun-cast P3HT:PCBM blends of composition (a) 33, (b) 41, (c) 70, and (d) 83 wt % PCBM. At 41 wt % the powder ring associated with PCBM is more intense than at 33 wt %, and equatorial scattering is significantly reduced. Higher concentration blends (c) and (d) show P3HT (010) scattering OOP (indicated with ←), not observed in pure P3HT, in addition to (100) scattering (indicated with →). The grazing angle was 0.14° and exposure time 50 s.

lattermost transition has a temperature well correlated with the transition we label B as observed after annealing pure PCBM (see below). The transitions marked C and D in Figure 3 are discussed below.

The thermal data show that significant changes occur upon increasing the PCBM concentration from 66 to 75 wt %. The glass transition drops sharply (between 70 and 75 wt %), and transitions (A, B) that we associate with pure PCBM are observed at concentrations above 75 and 66 wt %, respectively. These changes are strongly suggestive of a transition from a single phase below 70 wt % to a phase-separated state above 75 wt % PCBM. Phase-separated blends show characteristics of both pure PCBM and pure, or nearly pure, P3HT: i.e., the majority of the PCBM is no longer incorporated with the P3HT and forms a separate phase. The glass transition temperature of the P3HT-rich phase indicates that it has low PCBM content, as T_g is lower than that determined for the 66 wt % single phase.

In this context the phase separation is that which is occurring on the length scale measurable by the DMTA Instruments and may not represent the nanoscale phase separation sometimes observed in devices. Nonetheless, the phase-separated state at high PCBM loadings is a potentially important element in explaining the poor performance of devices with high PCBM loadings. More importantly, the increase in the bulk T_g will be important for defining effective thermal annealing treatments, as below T_g, morphological development will be hindered.

Clearly there are some differences between the data presented here and previously reported phase diagrams.[16,20,23] Our data show a rise in the glass transition temperature with PCBM content up to 70 wt %, while Zhao et al. observed a continuous rise of T_g with PCBM weight fraction across the entire composition range. We believe that the disparity is in part due to the difference in preparation method necessitated by the use of DSC: most crucially, the high-temperature treatment prior to thermal analysis. Melting of the blend will have occurred during the high-temperature phase, with the structural ordering at that temperature frozen in when the sample was quenched. Thus, while the high-temperature pretreatment indicates that there is no liquid−liquid separation of these materials in the melt, this is of limited relevance to the production of photovoltaic devices. Kim and Frisbie did observe the glass transition to increase with composition between 0 and 75 wt % PCBM but did not observe the glass transition above 75 wt %: a key indicator of the phase separation occurring in the blend.

While we do not observe the same eutectic nature as observed by Müller et al.,[23] we note that the temperature of recrystallization as reported by those authors (upon heating) is reduced significantly between 70 and 80 wt %. As the polymer's propensity to crystallize will be related to the mobility of the chain, the change in recrystallization temperature suggests that there is a significant change in the mobility of P3HT in the blend between 70 and 80 wt % PCBM. Our data show that the glass transition temperature of

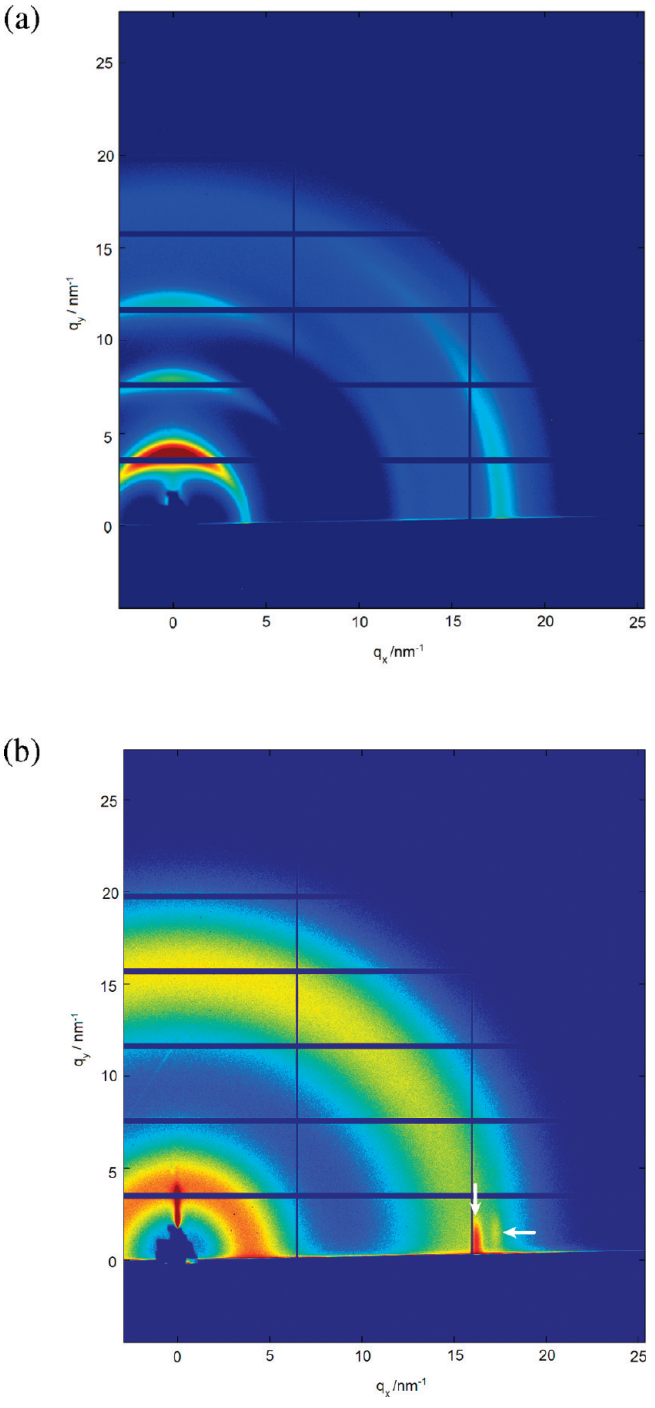

Figure 5. GIWAXS of pure P3HT cast from chlorobenzene: (a) as-cast; (b) after 60 min annealing at 210 °C. The grazing angle was 0.14° and exposure time 50 s. Note the in-plane features at $q_x = 16.4\ \mathrm{nm}^{-1}$ and $q_x = 17.1\ \mathrm{nm}^{-1}$ after annealing (indicated with ↓ and ←, respectively).

the blend is reduced by a similar amount (30−40 °C) over the same composition range and indicates the crossover from a single-phase to phase-separated mixture. With this interpretation, the recrystallization data of Müller et al. are consistent with our T_g data, indicating the onset of phase separation at 70 wt % PCBM.

2D GIWAXS images of spun-cast P3HT:PCBM blends are shown in Figure 4. At the lowest PCBM concentration (33 wt %, Figure 4a) scattering is predominantly from the P3HT

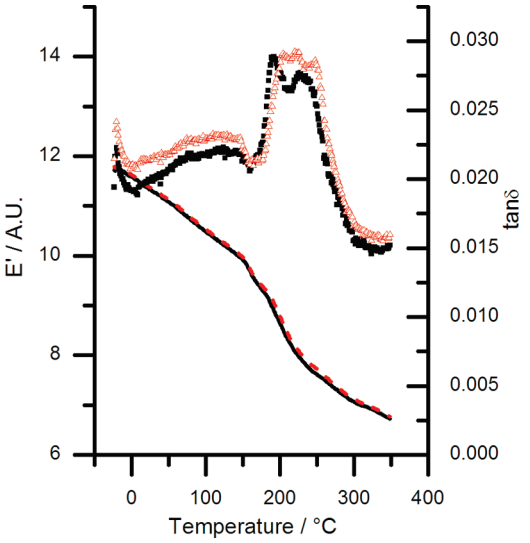

Figure 6. DMTA of pure solvent-cast PCBM after 60 min annealing at 132 °C. Transition B is observed as a drop in the elastic modulus at 155 °C, accompanied by a sharp increase in tan δ. 1.0 Hz: E', black line; tan δ, black squares. 10 Hz: E', red dashed line; tan δ, red triangles.

(GIWAXS image of pure P3HT is shown in Figure 5a), with a low-intensity ring associated with the PCBM (as-cast PCBM is shown in Figure 7a). At a PCBM concentration of 41 wt %, P3HT scattering is suppressed, particularly in-plane—the (010) reflection.

GIWAXS images of blends with a higher PCBM fraction (70 and 83 wt %, Figure 4, c and d, respectively) show an important difference to the low concentration blends: P3HT (010) scattering—which is predominantly in-plane for pure P3HT—is observed out-of-plane (OOP), in addition to the (100) scattering. This suggests that phase-separated regions within the film may be freed from the surface effects that result in the preferred orientation seen in the (single-phase) P3HT dominated films. Neutron scattering has shown depletion of PCBM at the free surface in 41 wt % blends.[14] If this is also true for higher wt % blends, the P3HT will likely be located at the free surface and will therefore be subject to different interfacial ordering effects. In two-phase blends, the P3HT-rich phase will be sitting atop a PCBM surface, whereas in the single-phase blends the mixed-component phase will interact with the underlying substrate, which may dominate the ordering throughout the rest of the film. Such differences are likely to be reflected in device performance.

Annealing of Pure Materials and Blends. In addition to working with the materials "as-cast", we have conducted annealing experiments to examine the effect on the transition of PCBM (and high PCBM fraction blends) at 155 °C and to investigate whether the liquid-crystalline state observed in pure P3HT is present in blended films. After annealing solvent-cast pure PCBM in the DMTA for 60 min at 132 °C and quenching, a reduction in the storage modulus is observed at 155 °C (Figure 6). It is reasonable to suggest that this is the same transition we observed in the phase-separated blends: the transition we have labeled (B), and consequently we have added this postannealing data from pure PCBM to our phase diagram. The origin of this transition is not clear, as a matched DSC experiment (data not shown here) does not indicate melting at this temperature (melting is observed at 244, 273, and 278 °C), although a change in the gradient of the heat flow is observed

dx.doi.org/10.1021/ma102524a |*Macromolecules* 2011, 44, 2908–2917

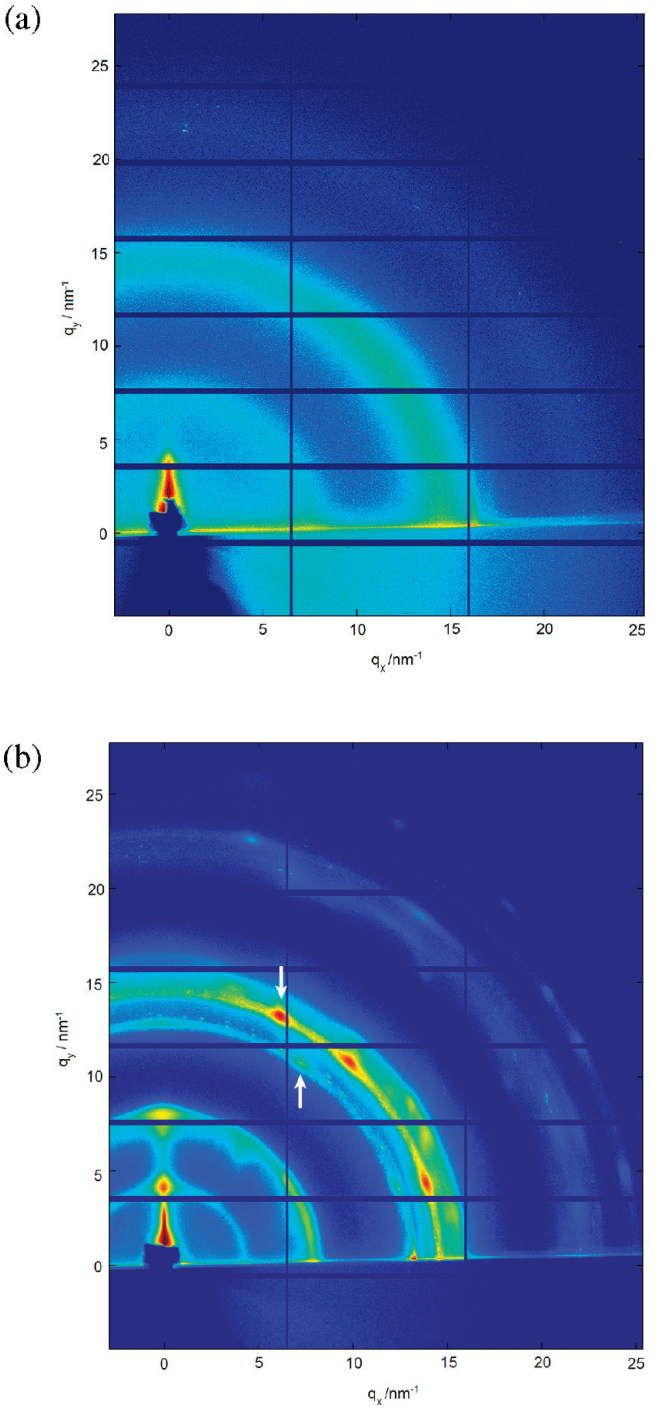

Figure 7. 2D GIWAXS images of pure solvent-cast PCBM: (a) as-cast; (b) after annealing for 60 min at 134 °C. The grazing angle was 0.15° and exposure time 50 s. After annealing scattering from a small number of large crystals with q-spacings of q = 15.0 nm^{-1} and q = 13.9 nm^{-1} is observed (radii indicated with ↓ and ↑, respectively), while prior to annealing the scattering reveals the sample to be highly polycrystalline.

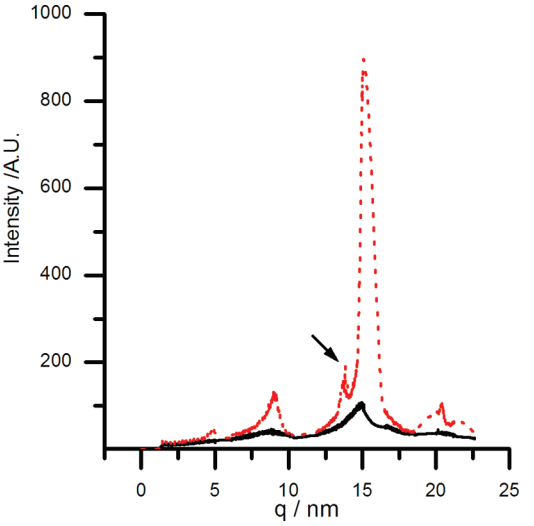

Figure 8. 1D cross sections (integrated over 8° wide sector centered 42° to the sample normal) of pure PCBM before (solid black line) and after (dashed red line) annealing at 134 °C. In addition to the increase in scattering at q = 15 nm^{-1}, after annealing a narrow peak is observed at q = 13.8 nm^{-1} (indicated with arrow).

at 121 °C. Transition B may be a solid−solid transition, but in absence of a clear signature from DMTA and DSC experiments, a positive identification is not possible.

Despite its unclear origin, this transition is a useful secondary indication of phase separation in blends, and the presence of a transition in the range commonly used for thermal annealing may have some impact on the design of thermal treatment for this and future material systems than include PCBM.

GIWAXS data for a pure PCBM film sample, prepared to complement the DMTA experiment, show considerable crystallization occurs during the annealing process (compare Figure 7, a and b, before and after annealing, respectively). The highest intensity signals in the annealed sample have approximately the same scattering vector (Q = 15 nm^{-1}) observed from amorphous PCBM scattering in the as-cast film. In addition, the annealed samples show a significant crystalline peak at Q = 13.8 nm^{-1}, indicating the formation of a second crystal population. Applying Scherrer analysis to the integrated intensity between 38° and 46° (Figure 8), we see that in as-cast PCBM the average crystal size for crystals with Q = 14.8 nm^{-1} is 2.66 ± 0.03 nm. The scattering data clearly show that the annealing at 132 °C has produced a small number of high perfection crystals: Scherrer analysis indicates crystal sizes of 10.1 ± 0.76 and 6.10 ± 0.04 nm for Q = 13.8 nm^{-1} and Q = 15.3 nm^{-1}, respectively. While the absolute values of the crystallite sizes depend upon the value of K used in the Scherrer relation (in this case we have used K = 0.93), the values do allow comparison of the crystallite sizes. The relatively large size of these crystallites, as measured by Scherrer analysis, suggests that the crystal phase which is the origin of this additional scattering peak is energetically favorable at 134 °C. The larger lattice spacing (0.91 nm compared to 0.85 nm prior to annealing) of the phase with the larger crystals may be indicative of a less stable phase, consistent with the relatively mild annealing conditions.

To reveal the further (higher temperature) melting transitions of pure PCBM by DMTA, it was necessary to enhance crystallinity by annealing. After 60 min at 240 °C, followed by quenching, a clear melting signature is observed by DMTA at 288 °C (see Figure 9a, labeled transition D on the figure). After slowly cooling this sample to ambient from 350 °C and repeating the DMTA thermal scan, a second melting transition is observed at 210 °C (Figure 9b, labeled C). The smaller tan δ peak associated with transition D in the slow cooled case is likely to

dx.doi.org/10.1021/ma102524a |*Macromolecules* 2011, 44, 2908–2917

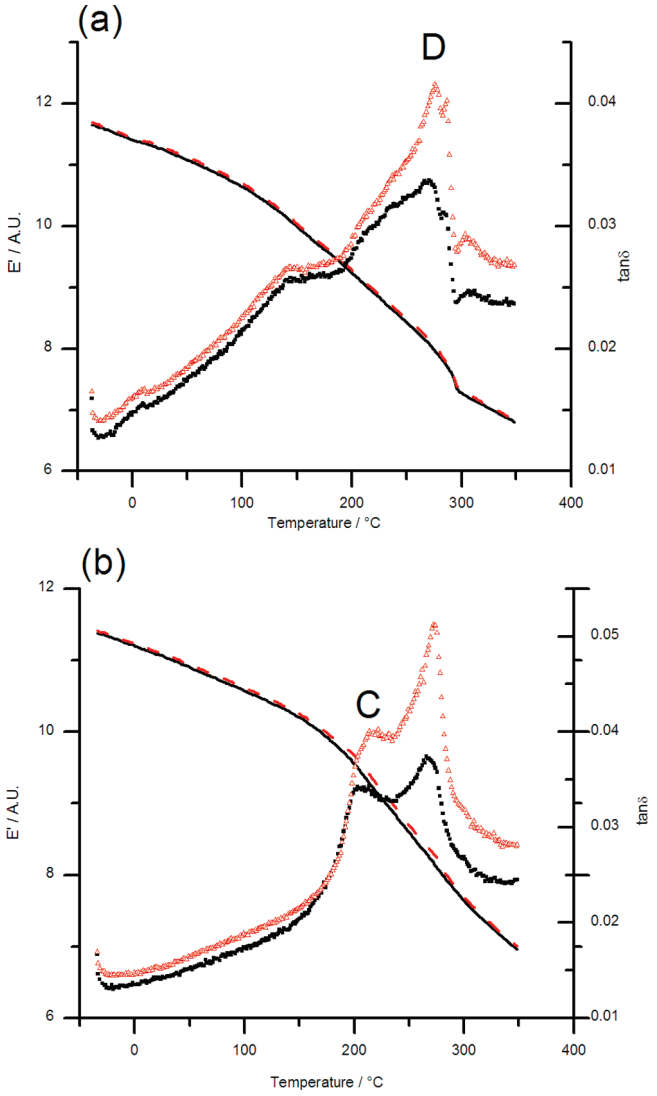

Figure 9. DMTA thermal scan of pure solvent-cast PCBM: (a) after 60 min annealing at 240 °C; (b) after slow cooling from 350 °C. Enhancements of the 278 °C (labeled D in text) and 207 °C (labeled C in text) peaks are observed in (a) and (b), respectively.

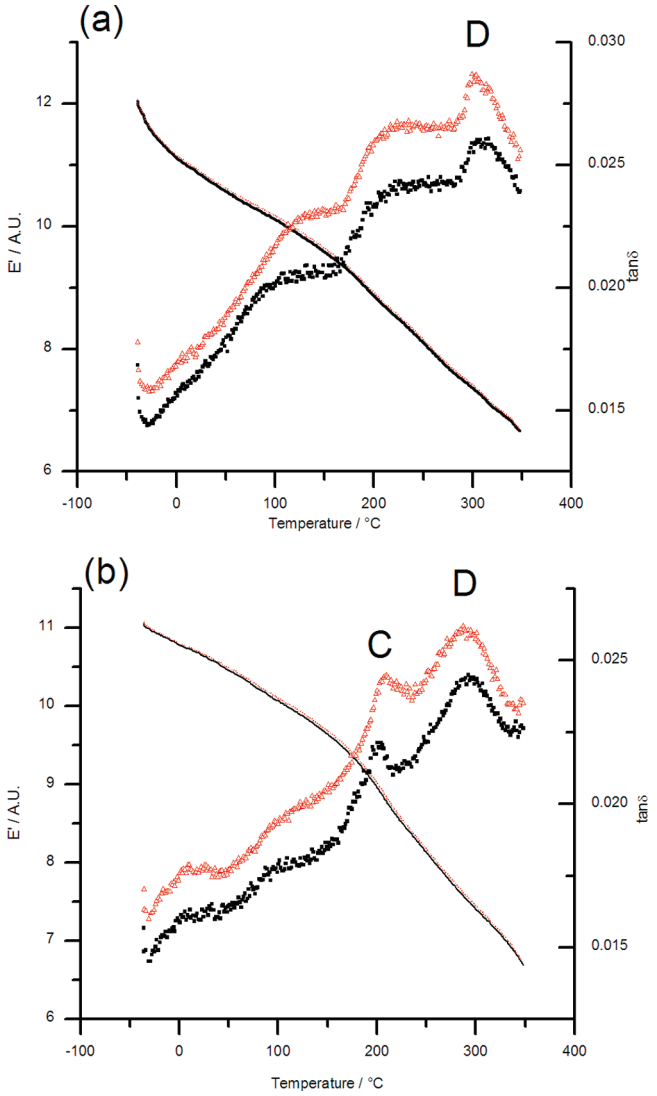

Figure 10. DMTA thermal scans of 83 wt % PCBM in P3HT after (a) annealing at 265 °C for 60 min and quenching (b) and slow cooling from 350 °C. Enhancement of transition D is predominant in (a) and transition C in (b). Slow cooling enhances crystal population C.

be due to a smaller population of lower quality crystals of this phase, as compared to the annealed and quenched sample.

Annealing and slow cooling experiments with an 83 wt % PCBM in P3HT blend leads to the transitions C and D shown in Figure 10, although transition D is suppressed in the blend compared to the pure PCBM—as seen by the smaller peak in tan δ. The addition of P3HT apparently disrupts the cold crystallization of the phase with melting transition D during the annealing process. These transitions have also been included in Figure 3.

GIWAXS data of spun-cast pure P3HT films before and after annealing for 60 min at 210 °C are shown in parts a and b of Figure 5, respectively. While the OOP diffraction features—partially obscured by the gaps in the detector—seen in the as-cast film are not present after annealing, strong in-plane features are observed. The as-cast film shows a single strong peak at Q = 17.3 nm^{-1} (d-spacing 0.363 nm), with the film annealed at 210 °C showing in-plane features at Q = 16.4 nm^{-1} and Q = 17.1 nm^{-1} (d-spacings of 0.384 and 0.367 nm, respectively). Applying Scherrer analysis to the peaks indicates that the in-plane diffraction features are due to crystalline regions of average size of 9 nm for the as-cast film and 17−18 nm for the film annealed at 210 °C.

Similarly treated blend films with compositions of 33 and 41 wt % PCBM also show in-plane ordering of P3HT after thermal annealing at 210 °C (Figure 11a,b), with d-spacings of 0.382 and 0.383 nm for 33 and 41 wt %, respectively. Scherrer analysis gives crystal sizes of 29 and 24 nm for 33 and 41 wt %, respectively. These data show that samples quenched from between the two P3HT melting transition temperatures have order perpendicular to the substrate while other ordering is absent, further suggesting a liquid-crystal phase (with spacing 0.383 nm persistent over 18 nm). Further, ordering in the liquid-crystal phase is not significantly altered by the addition of up to 41 wt % PCBM, with lattice spacing of ~0.383 nm persistent over 18−29 nm.

As our thermal data were obtained from samples that have a thermal history more akin to organic photovoltaic devices than previously reported studies, we believe that our phase diagram

dx.doi.org/10.1021/ma102524a |*Macromolecules* 2011, 44, 2908–2917

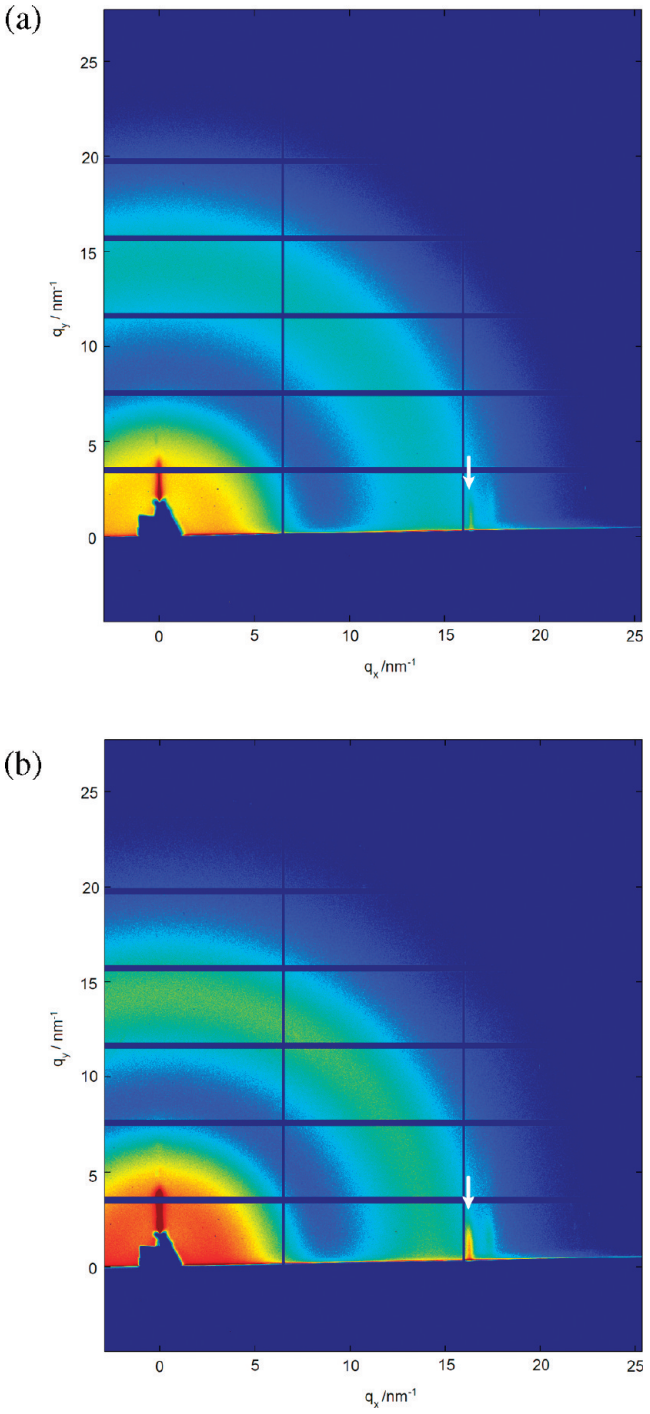

Figure 11. GIWAXS from (a) 33 wt % and (b) 41 wt % blends after annealing for 1 h at 210 °C and quenching. Note the in-plane scattering both cases (indicated with ↓), as in pure P3HT (Figure 5).

will be helpful in understanding the phase separation effects at the onset of annealing. The rise in T_g with PCBM content—implying that PCBM is an antiplasticizer for P3HT—has an important implication for device processing: the T_g of the blend determines a minimum effective temperature for annealing, as below the T_g the crystallinity of the P3HT will not improve. Furthermore, the glass transition determines the stability of the device morphology—devices or phase-separated regions with PCBM compositions below 33 wt % will be metastable, so the thermal loading inevitable in operation will result in (undesirable) changes in morphology.

The phase diagram we present facilitates a rational approach to the design of thermal annealing treatments for organic photovoltaics: enhancement of P3HT crystallinity—for enhanced charge transport—will only be achieved by annealing above the blend composition glass transition temperature. We believe that the observation of cold crystallization at 132 °C is a likely explanation for the crystallites commonly observed in thermally annealed devices.[2,30] The observation of such crystallites in devices with an approximately equal blend ratio after annealing indicates that the P3HT/PCBM single phase is not thermodynamically stable at the annealing temperature (which is inevitably above the blend T_g). Investigation of the kinetics of this process may allow processing routes to be devised for this system that reduce the growth of these crystallites, which are still above the T_g of the blend. The importance (if any) of the liquid-crystal phase of P3HT, and low PCBM wt % blends, to devices is not yet clear; if the PCBM is intercalated[31,32] with the P3HT, this may enhance exciton dissociation, but electron transport will be poor if percolation paths do not exist between the PCBM molecules.

CONCLUSIONS

Using DMTA, we have measured the glass transition for P3HT:PCBM blends across the composition range. We have observed a mechanical transition of PCBM at 155 °C in both pure material and blends with greater than 66 wt % PCBM. Crucially this transition occurs within the temperature range commonly used for solar cell annealing. Both of these transitions indicate that in an as-cast state below 70 wt % PCBM there exists a single phase. However, at high PCBM weight fraction, the blend separates into two phases. The finding of phase separation and cold crystallization has implications for the design of processing treatments, as does the finding of significant hygroscopicity in PCBM.

EXPERIMENTAL SECTION

P3HT was purchased from Sigma-Aldrich (produced by Rieke Metals) with a specified regioregularity of >98%, and used as received. Material from this batch has been used to produce efficient (4.4% PCE) devices.[33] PCBM was purchased from Solenne and was dried at 100 °C and reduced pressure (<10 mbar) for 1 h prior to solution preparation (with the exception of the TGA measurements, where the powder was used as received). Characterization of the P3HT molecular weight distribution was carried out by MALDI-TOF mass spectrometry using an ABI 4700 Proteomics analyzer running in linear mode with dithranol as the matrix[24] and a Polymer Laboratories PL-GPS 50 with chloroform as the solvent. Thermogravimetric analysis was carried out using a TA Instruments TGA Q500, heating at 10 °C/min and purged with nitrogen at 60 mL/min.

Pure materials were dissolved in chlorobenzene (BDH Limited, Poole, UK, 99.5%) at a concentration of 50 mg/mL and heated to 70 °C to ensure the material was completely dissolved and free from "nanowires" of P3HT.[34,35] Blend solutions were prepared from these hot solutions by mixing the pure component solutions by volume. These solutions were subsequently reheated to 70 °C immediately prior to use. This preparation route is matched to the preparation route used for the production of photovoltaic devices.[36]

For DMTA analysis of as-cast P3HT:PCBM blends, films were drop-cast (typically about 40 μL) onto cleaned (distilled water, acetone, isopropyl alcohol) stainless steel "material pockets"[37] and dried under continuous N_2 flow. The pockets were subsequently closed by folding in half along the long axis, thus enclosing the film. The sample was then transferred to the DMTA (Tritec 2000 dynamic mechanical analyzer, Triton Technology, Nottinghamshire, UK) and rapidly cooled to below −30 °C using liquid nitrogen purging of the sample oven. For analysis of as-received powders, 5−10 mg of powder was clamped within the "material pocket". The DMTA was operated in single cantilever bending mode, with a free length of 10 mm and an oscillating strain of 1%. Strain frequencies from 0.1 to 100 Hz were used to aid the identification of the glass transition, with the 1 Hz data used for analysis. Heating of the sample in the DMTA was typically conducted at 5 °C min^{-1}, with the sample oven continuously purged with nitrogen gas throughout. Fresh samples were prepared for each DMTA experiment, with the exception of the annealing experiments, where samples were first subjected to a data collection scan. Annealing for DMTA experiments was carried out in situ in the DMTA oven, quenching the sample by flushing the DMTA oven with both liquid nitrogen and chilled gaseous nitrogen—achieving initial cooling rates of ∼100 °C min^{-1}.

For grazing incidence wide-angle X-ray scattering (GIWAXS), a 1 mm thick silicon wafer was cleaved to 10 mm × 10 mm and cleaned for 20 min with an ultraviolet cleaner (Novascan PSD-UVT). 35 μL of blend solutions was spun-cast onto the Si wafer pieces spinning at 1200 rpm and spun until dry. The samples were annealed on a preheated hot plate for 60 min in air, after which the samples were immediately quenched into liquid nitrogen. GIWAXS experiments were carried out at the I16 beamline at the Diamond Light Source (Harwell, UK), using a beam energy of 10 keV, and a Dectris Pilatus 2M detector. The custom end chamber used on the beamline was fabricated in-house and was equipped with an entrance slit and an internal beamstop to prevent beam scattering by the Kapton exit window. Scatter within the chamber was further reduced by a continuous purge with helium gas. The Pilatus data were analyzed using in-house written MATLAB software.

■ ASSOCIATED CONTENT

Ⓢ Supporting Information. TGA of pure PCBM powder (Figure S1); DMTA thermal scans of P3HT:PCBM blends at 33, 50, and 83 wt % PCBM (Figures S2−S4). This material is available free of charge via the Internet at http://pubs.acs.org.

■ AUTHOR INFORMATION

Corresponding Author

*E-mail: peh26@cam.ac.uk (P.E.H.); amd3@cam.ac.uk (A.M.D.).

■ ACKNOWLEDGMENT

Thanks to John Gearing of Gearing Scientific for his assistance with the DMTA equipment and introduction to DMTA data interpretation. TGA was carried out with the assistance of Robert Cornell at the Polymer Characterization Laboratory, Department of Materials Science, University of Cambridge. MALDI-MS was carried out by Asha Boodhun at the Department of Chemistry, University of Cambridge. Thanks to Gareth Nisbet at beamline I16, Diamond Light Source, for providing invaluable assistance during our beamtime. The UKOPV collaboration thanks the EPSRC for financial support via grant "Optimization of polymer photovoltaic devices through control of phase separation" (Grant references EP/F016433/1, EP/F016255/1, EP/F017057/1, and EP/F019297/1).

■ REFERENCES

(1) Brabec, C. J. *Sol. Energy Mater. Sol. Cells* **2004**, *83*, 273–292.
(2) Campoy-Quiles, M.; Ferenczi, T.; Agostinelli, T.; Etchegoin, P. G.; Kim, Y.; Anthopoulos, T. D.; Stavrinou, P. N.; Bradley, D. D. C.; Nelson, J. *Nature Mater.* **2008**, *7*, 158–164.
(3) Swinnen, A.; Haeldermans, I.; Vanlaeke, P.; D'Haen, J.; Poortmans, J.; D'Olieslaeger, M.; Manca, J. V. *Eur. Phys. J.: Appl. Phys.* **2006**, *36*, 251–256.
(4) Vanlaeke, P.; Swinnen, A.; Haeldermans, I.; Vanhoyland, G.; Aernouts, T.; Cheyns, D.; Deibel, C.; D'Haen, J.; Heremans, P.; Poortmans, J.; Manca, J. V. *Sol. Energy Mater. Sol. Cells* **2006**, *90*, 2150–2158.
(5) Guo, T.-F.; Wen, T.-C.; L'Vovich Pakhomov, G.; Chin, X.-G.; Liou, S.-H.; Yeh, P.-H.; Yang, C.-H. *Thin Solid Films* **2008**, *516*, 3138–3142.
(6) Gang, L.; Shrotriya, V.; Yan, Y.; Jinsong, H.; Yang, Y. *J. Mater. Chem.* **2007**, *17*, 3126–3140.
(7) Li, G.; Shrotriya, V.; Huang, J. S.; Yao, Y.; Moriarty, T.; Emery, K.; Yang, Y. *Nature Mater.* **2005**, *4*, 864–868.
(8) Kim, Y.; Cook, S.; Tuladhar, S. M.; Choulis, S. A.; Nelson, J.; Durrant, J. R.; Bradley, D. D. C.; Giles, M.; Mcculloch, I.; Ha, C. S.; Ree, M. *Nature Mater.* **2006**, *5*, 197–203.
(9) Ma, W. L.; Yang, C. Y.; Gong, X.; Lee, K.; Heeger, A. J. *Adv. Funct. Mater.* **2005**, *15*, 1617–1622.
(10) Kline, R. J.; McGehee, M. D.; Kadnikova, E. N.; Liu, J. S.; Frechet, J. M. J.; Toney, M. F. *Macromolecules* **2005**, *38*, 3312–3319.
(11) Yang, X.; Loos, J.; Veenstra, S. C.; Verhees, W. J. H.; Wienk, M. M.; Kroon, J. M.; Michels, M. A. J.; Janssen, R. A. J. *Nano Lett.* **2005**, *5*, 579–583.
(12) Klimov, E.; Li, W.; Yang, X.; Hoffmann, G. G.; Loos, J. *Macromolecules* **2006**, *39*, 4493–4496.
(13) Savenije, T.; Kroeze, J.; Yang, X.; Loos, J. *Adv. Funct. Mater.* **2005**, *15*, 1260–1266.
(14) Parnell, A. J.; Dunbar, A. D. F.; Pearson, A. J.; Staniec, P. A.; Dennison, A. J. C.; Hamamatsu, H.; Skoda, M. W. A.; Lidzey, D. G.; Jones, R. A. L. *Adv. Mater.* **2010**, *22*, 2444–2447.
(15) Kim, Y.; Choulis, S. A.; Nelson, J.; Bradley, D. D. C.; Cook, S.; Durrant, J. R. *Appl. Phys. Lett.* **2005**, 86.
(16) Kim, J. Y.; Frisbie, C. D. *J. Phys. Chem. C* **2008**, *112*, 17726–17736.
(17) Hugger, S.; Thomann, R.; Heinzel, T.; Thurn-Albrecht, T. *Colloid Polym. Sci.* **2004**, *282*, 932–938.
(18) Swinnen, A.; Zhao, J.; Van Assche, G.; Vanderzande, D.; D'Olieslaeger, M.; Manca, J. V.; Van Mele, B. In *Organic Photovoltaics Viii*; Kafafi, Z. H., Lane, P. A., Eds.; Proceedings of the Society of Photo-Optical Instrumentation Engineers (Spie); Spie-Int Soc Optical Engineering: Bellingham, 2007; Vol. 6656, pp 65619−65619.
(19) Zhao, Y.; Yuan, G. X.; Roche, P.; Leclerc, M. *Polymer* **1995**, *36*, 2211–2214.
(20) Zhao, J.; Swinnen, A.; Van Assche, G.; Manca, J.; Vanderzande, D.; Mele, B. V. *J. Phys. Chem. B* **2009**, *113*, 1587–1591.
(21) Kuila, B. K.; Nandi, A. K. *Macromolecules* **2004**, *37*, 8577–8584.
(22) Kuila, B. K.; Nandi, A. K. *J. Phys. Chem. B* **2006**, *110*, 1621–1631.
(23) Müller, C.; Ferenczi, T. A. M.; Campoy-Quiles, M.; Frost, J. M.; Bradley, D. D. C.; Smith, P.; Stingelin-Stutzmann, N.; Nelson, J. *Adv. Mater.* **2008**, *20*, 3510–3515.
(24) Liu, J. S.; Loewe, R. S.; McCullough, R. D. *Macromolecules* **1999**, *32*, 5777–5785.
(25) Nien, Y. H.; Chen, S. H.; Chen, J. W. *J. Appl. Polym. Sci.* **2010**, *117*, 2839–2846.
(26) Silberstein, M. N.; Boyce, M. C. *J. Power Sources* **2010**, *195*, 5692–5706.
(27) Prosa, T. J.; Winokur, M. J.; Moulton, J.; Smith, P.; Heeger, A. J. *Macromolecules* **1992**, *25*, 4364–4372.
(28) Qian, R. Y.; Chen, S. X.; Song, W. H.; Bi, W. P. *Macromol. Rapid Commun.* **1994**, *15*, 1–6.
(29) Rispens, M. T.; Meetsma, A.; Rittberger, R.; Brabec, C. J.; Sariciftci, N. S.; Hummelen, J. C. *Chem. Commun.* **2003**, 2116–2118.

(30) Reyes-Reyes, M.; Lopez-Sandoval, R.; Arenas-Alatorre, J.; Garibay-Alonso, R.; Carroll, D. L.; Lastras-Martinez, A. *Thin Solid Films* **2007**, *516*, 52–57.
(31) Reyna-Valencia, A.; Deyrail, Y.; Bousmina, M. *Macromolecules* **2010**, *43*, 354–361.
(32) Vaia, R. A.; Giannelis, E. P. *Macromolecules* **1997**, *30*, 8000–8009.
(33) Kingsley, J.; Green, A.; Lidzey, D. *Proc. SPIE* **2009**, *7416*, 74160T−1–74160T−9.
(34) Berson, S.; De Bettignies, R.; Bailly, S.; Guillerez, S. *Adv. Funct. Mater.* **2007**, *17*, 1377–1384.
(35) Kim, D. H.; Park, Y. D.; Jang, Y.; Kim, S.; Cho, K. *Macromol. Rapid Commun.* **2005**, *26*, 834–839.
(36) Manuscript in preparation.
(37) Tg and Melting Point of a Series of Polyethylene Glycols Using the Material Pocket, Application Note, Perkin-Elmer, Waltham, MA.